DOI 10.1007/s10891-021-02328-3
Journal of Engineering Physics and Thermophysics, Vol. 94, No. 3, May, 2021

HEAT AND MASS TRANSFER IN DISPERSED AND POROUS MEDIA

ON THE POTENTIAL OF THE MIE THEORY AND THE SIMULATION APPROACH IN INVESTIGATING SPECTRAL-KINETIC COEFFICIENTS OF ULTRAPOROUS THERMAL PROTECTIVE MATERIALS

V. V. Cherepanov and O. M. Alifanov

UDC 537.87

Certain capabilities of the original combined statistical simulation mathematical model covering the structure and physical properties of fibrous and reticulated high-temperature materials have been shown. An important element of the model is a "virtual scanner" developed earlier, i.e., a software tool making it possible to investigate the pattern of interaction between electromagnetic radiation and orthogonal representative elements of materials. Free parameters have been described and tests of both the spectral part of the model based on the Mie theory and the joint model, which confirm their adequacy, have been presented. The behavior of local spectra of transmission, absorption, and scattering of electromagnetic radiation of a number of the existing and hypothetical materials has been studied. In certain reticulated materials, the authors recorded an "order catastrophe" in the absorption spectrum: an abrupt and strong, of several orders of magnitude, change in the spectral absorption coefficients, that is not associated with resonance phenomena in absorption. The presence of a fairly wide resonance region was recorded in the transmission spectrum of an amorphous-quartz-based fibrous material and the parameter affecting the location of this region was found.

Keywords: *high-temperature porous materials, radiation spectral-kinetic coefficients, modeling, phase transitions.*

Introduction. Open-porosity materials, fibrous materials, and reticulated foams are widely used in medicine, civil engineering, metallurgy, the chemical and food industries, power engineering, automobile production, and other branches of the national economy. In the aerospace and aviation industry, the lightest of these materials, i.e., ultraporous nonmetallic materials (Figs. 1 and 2), are traditionally used for thermal protection and sound and noise proofing. In recent times, new advanced fields of application have appeared for such materials because of the development of production and modification technologies [1, 2]

Many physical properties of ultraporous nonmetallic materials cannot be experimentally measured directly. Their indirect determination is implemented by solution of inverse problems, direct modeling, or identification of the parameters of mathematical models of physical processes occurring in the materials′ volume [3–14]. Models of materials that are used in investigating heat transfer are either analytical heuristic continuous or discrete numerical-simulation type [6–9]. Models of the first type are much more simply integrated into the analytical apparatus of inverse identification problems. However, the capabilities of computer discrete models are considerably wider; they enable us to take a fuller account of the distinctive features of individual materials and to calculate and investigate a broader spectrum of their physical properties on a rigorous basis.

In substances used in the production of thermal protective materials and coatings, the intrinsic thermal conductivity is usually relatively low and depends weakly on temperature. Electromagnetic radiation penetrates deep into the volume of ultraporous materials, and their radiative thermal conductivity, in contrast to the intrinsic thermal conductivity, grows quite rapidly with temperature [6, 8, 15, 16]. Therefore, heat transfer at comparatively high temperatures in such materials is mainly by radiation. Nonetheless, many important characteristics of the process of transfer of radiation whose values are spectrally dependent and/or are formed at a microlevel have been beyond the scrutiny of researchers to date. This is

Moscow Aviation Institute (National Research University), 4 Volokolamskoe Highway, Moscow, 125993, Russia; email: vvcherepanov@yandex.ru, o.alifanov@yandex.ru. Translated from Inzhenerno-Fizicheskii Zhurnal, Vol. 94, No. 3, pp. 566–577, May–June, 2021. Original article submitted November 21, 2020.

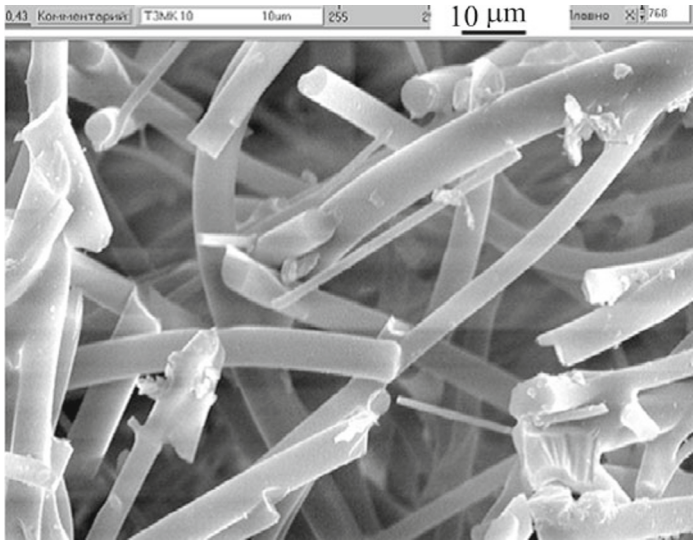

Fig. 1. Microstructure of fibrous material TZMK-10.

true of the parameters of complex media involved in the kinetic equation of radiation transfer: of spectral absorption and scattering coefficients and the scattering indicatrix absolutely unexplored in multiphase media with complex morphology. This status of the problem, in particular, with the indicatrix, is largely attributed not only to its tedious determination, but also to the fact that in a number of heat-transfer problems solvable for such media, difficulties with determining the real indicatrix may be avoided by using some model distributions or others [15, 16]. For this reason, e.g., in the problems of radiative heat transfer, a transport approximation is frequently used for homogeneous materials [16]. This is due to the fact that the macroscopic energy equation obtained from the kinetic radiation transfer equation by integrating with respect to directions and frequencies does not depend explicitly on the indicatrix, since the contribution of the scattering integral, where it is involved, to such an energy equation is equal to zero [15]. At the same time, the radiation state can also affect the results of calculating the spectral-kinetic coefficients of this equation. Also, it is well known that, strictly speaking, the macroscopic boundary conditions are not correct everywhere in contrast to the kinetic conditions. In particular, the validity of macrodescription is violated near the boundaries of the domain. Therefore, the approach based on the energy equation and the model indicatrices used may produce significant errors in the problems of radiative heat transfer in the immediate vicinity of structural elements, structural defects, etc. Such problems require correct boundary conditions and kinetic description, and the scattering indicatrix is necessary to solve them. Certainly, there can be other applications for it. However, until recently, there has been no efficient tool for calculating the scattering indicatrix.

In [12], we described a spectral model making it possible to reproduce and investigate a continuous spatial pattern of scattering of electromagnetic radiation on such optically complex physical objects, as orthogonal representative elements (OREs) consisting, e.g., of orthogonal cylinders and, probably, a sphere. This enabled us to construct a "virtual scanner:" a software tool to investigate both the scattering and absorption spectra of OREs and their spectral scattering indicatrix.

The model is based on the following quite traditional assumptions:

1) On a spatial scale of the order of fractions of a micron or higher, the components of the incident field and of the field scattered by the fragments of material are linked by the relations of strict electromagnetic theory or, sometimes, of its particular corollary: the scalar theory of diffraction [18, 19].

2) The electromagnetic wave incident on the representative element of the material is scattered singly, elastically, and independently by its fragments in accordance with the Mie theory. In particular, the radiation scattered by one fragment is disregarded in the radiation incident on the remaining fragments of the representative element in question and other OREs.

3) Dimensions of the fragments of the material and local properties of radiation are taken into account. The medium into which the material′s fragments are submerged does not absorb electromagnetic radiation.

4) The optical characteristics of the material′s volume element associated with the OREs are determined by averaging the characteristics of individual fragments with weights proportional to their cross sections in the processes of absorption and scattering of radiation.

Studies [8, 11] gave statistical mathematical models of the structure and physical properties of ultraporous fibrous and reticulated nonmetallic materials into which the above-described optical model was integrated. Studies [13, 14] implemented the approach with simulation-modeling elements in investigating heat transfer in heat-resistant quartz ceramics partially transparent to electromagnetic radiation. It turned out that the use of such combined extended models enables us to take account of and to investigate a rather broad spectrum of processes and properties of materials. Construction of the combined models was carried out according to the following key rules:

1) The material is replaced, in modeling, by a stochastic system of representative elements [12] which are generated and analyzed successively.

2) Account is taken of the effective density and anisotropy of the material, and also of the statistical regularities of its structure, the presence of additional thermal and electrical resistances of the region of contact of fragments and of floccules in the base structure, and of the properties of substances forming the material′s base.

3) In calculating thermal conductivity, use is made of isothermal and adiabatic approximations within the limits of each separate representative element [8]. The effective complex permittivity is calculated in an electrostatic approximation [18].

4) Each new representative element is considered to be submerged in an effective medium whose thermophysical properties are also determined by all the elements generated before [8, 11].

5) To determine the optical-radiative properties of the material, use is made of both the classical electromagnetic theory and quantum optics. Thus, in calculations, we can use radiation-intensity models and dependences obtained by solution of kinetic radiation-transfer models alike.

6) Local optical-radiative characteristics of the material are determined within the framework of a modified optical model. It is based on the above-described model of interaction with the radiation of individual representative elements but contains, in particular, a tool for introducing cooperative corrections into the results of radiation scattering by individual fragments of the material.

The developed models possess a certain number of "degrees of freedom" and contain free numerical and functional parameters to be determined in the course of the procedure of identifying them by the data obtained at the preliminary steps of investigation. For this purpose, use is made of the apparatus of solving inverse problems using, as the initial data, results of an optical [13] or nonstationary thermal experiment [5, 20]. On the basis of the models, a software tool was developed that makes it possible to carry out the calculations and also to investigate and predict many important properties of ultraporous nonmetallic materials. The package software was written in the Matlab language. In the proposed work, we give results of investigating, with it, the local optical-radiative properties of a number of the existing and hypothetical materials. The modeling was carried out on different computers. Therefore, we used both a 32-bit Matlab version and a 64-bit version, with the system′s software being thoroughly tested.

Monitoring the Operation of Distribution Generators and Key Programs of the Mie Theory. In developing software, use was made of the well-known approved methods and algorithms, where possible. The standard Matlab program was used as the generator of pseudorandom numbers distributed uniformly on the segment [0, 1]. Pseudorandom numbers having a nonuniform distribution on the segment were obtained using the numbers distributed uniformly on [0, 1]. In particular, we employed a rather simple von Neumann method based on the following statement [21, 22]:

Let $0 \le \psi(x) \le M$ *be defined on the segment* $[a, b]$. Then, if ζ and y are independent random quantities distributed uniformly on [0, 1] and $[a, b]$ respectively, the density of the conditional distribution $P\{y \le x \mid \psi(y) \ge M\zeta\}$ coincides with $C\psi(x)$, where C is the normalization constant.

It follows from the statement that for the necessary law of distribution of the quantity y to be obtained, the process of generation of pairs of random values of ζ and ρ distributed uniformly on [0, 1] should be continued until the inequality $\psi(y) \ge M\zeta$, where $y = a + (b - a)\rho$, holds true. It turned out that this method is also conveniently used where the distribution is assigned by a piecewise-continuous function, e.g., by a histogram. We also know modifications of this method that possess higher efficiency.

The Henji–Greenstein distribution [15, 16, 23]

$$\psi_{\mathrm{HG}}(y|g) = 0.5(1 - g^2)(1 + g^2 - 2yg)^{-3/2}, \quad g = \langle y \rangle = \int_{-1}^{1} y\psi_{\mathrm{HG}}(y|g)dy, \tag{1}$$

on the segment [–1, 1], which is of rather frequent use in quantum optics, like a number of other distributions with a comparatively simply integrated probability density, can be obtained using the inversion formulas (Smirnov transformation) following from the assumptions:

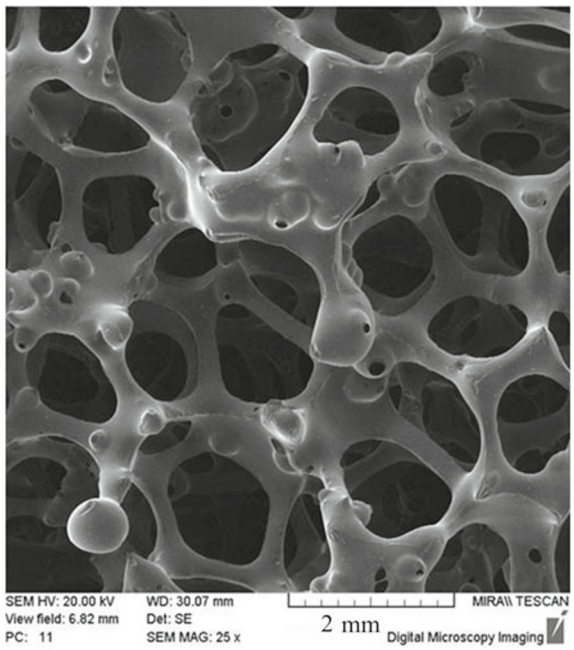

Fig. 2. Microstructure of SiC-coated reticulated vitreous carbon RVC.

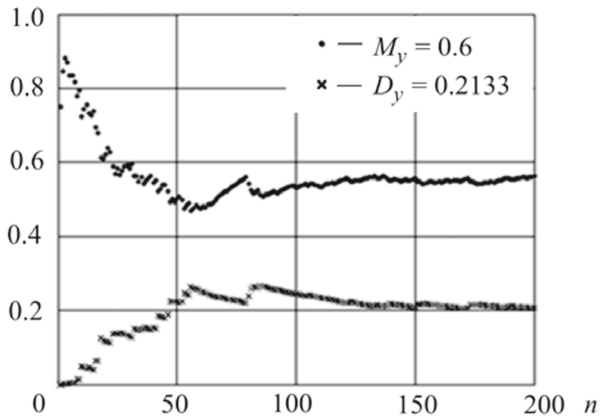

Fig. 3. Typical plots of M and D vs. number n of elements of a pseudorandom sequence with a probability density (1). The von Neumann method was employed. The accurate distribution parameters are $M_y = 0.6$ and $D_y = 0.2133$.

If the random quantity y satisfies the equation

$$\int_{-\infty}^{y} dF(x) = \int_{-\infty}^{y} \psi(x)dx = \zeta \in [0, 1] \text{ or } y = F^{-1}(\zeta) , \tag{2}$$

in which ζ is the uniformly distributed random quantity, then y has the distribution law $F(x)$ and the density $\psi(x)$.

The method enables us to directly express the quantity with a required distribution law by the quantity distributed on [0, 1] uniformly. In particular, upon integrating (2), we obtain, for the distribution (1),

$$y = [1 + g^2 - ((1 - g^2)/(1 + g - 2g\zeta))^2]/(2g) . \tag{3}$$

Distribution sensors operating by these algorithms were pretested for the correctness of first distribution moments: the mathematical expectation M and the dispersion D (Fig. 3). In all the cases, the generated sequences possessed necessary

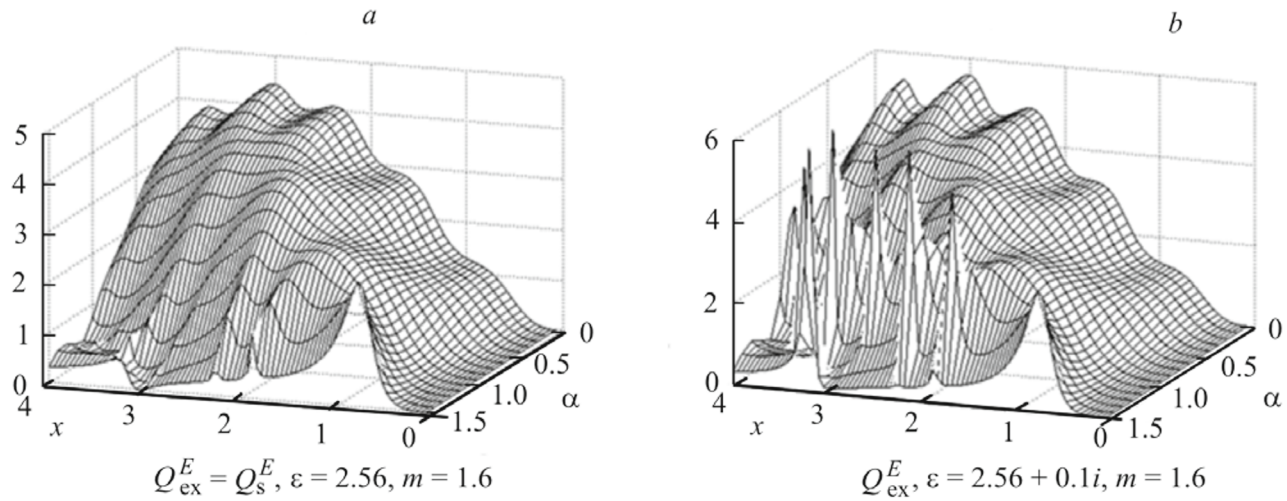

Fig. 4. Efficiencies of attenuation and scattering of infinite homogeneous straight circular cylinders vs. angle of incidence $\alpha \in [0, 0.5\pi]$ and diffraction parameter $x \in [0, 4]$.

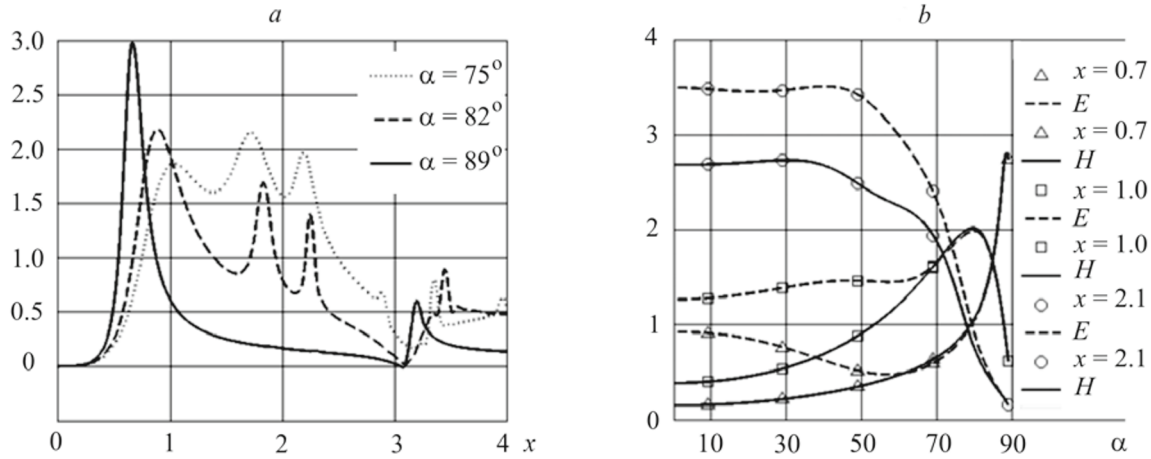

Fig. 5. Efficiencies of extinction of an infinitely long cylinder vs. diffraction parameter $x = kR$ (a) and angle of incidence α (b) at the relative refractive index $m = 1.6$ ($\varepsilon = 2.56$ and $\mu = 1$).

characteristics with a sufficient sample volume. Thus, in the above example, a sample volume of approximately 10^4 values guaranteed that M and D of the sample differ from their exact values no more than in the third significant figure irrespective of the development of the initial step of generation.

In the relations of the Mie theory for a sphere and a cylinder, the Bessel and Hankel functions involved in them, and also their logarithmic derivatives, were computed in iterative sequences suppressing computational instabilities. The principle of construction of these sequences has been described in [19] in detail. The values of the Bessel and Hankel functions, obtained in this manner, were compared with the results of the standard Matlab software, which computed analogous values by the method of summation of relevant series. The coincidence of the results of operation of different programs for the values of double exactness, which is used in Matlab by default, was stable up to and including the 15th significant figure, i.e., up to the figures, in practice, whose values may be affected by the roundoff errors of the processor in the 64-bit version.

The most important programs of the system are the tools describing the interaction between basic fragments of representative elements, i.e., a sphere and a cylinder, and electromagnetic radiation. This software was thoroughly tested.

The results of its operation were compared with the reported results of calculating both the elements of the amplitude scattering matrix and efficiencies and the coefficients of scattering series by which these quantities are expressed in the Mie theory [14–16]. The results of testing fully confirmed the correctness of operation of this software and the possibility of applying it to mathematical modeling of spectral properties.

Figures 4 and 5 give results of calculating the efficiencies of arbitrarily illuminated homogeneous infinitely long straight circular cylinders, which can be used for comparison with the data reported in [24]. Figure 4 shows the dependences of the attenuation and scattering efficiencies calculated for the cylinders with $\varepsilon = 2.56$ and $\varepsilon = 2.56 + 0.1i$ from the formulas of [24] for the values of the angle of incidence $\alpha \in [0, 0.5\pi]$ and the diffraction parameter $x \in [0, 4]$.

The variant of polarization of the incident radiation is denoted by a superscript [19, 24]. In the figures, we can clearly see the resonance regions noted in [24] in the process of scattering and attenuation, which are formed at small angles of slip of the incident radiation. Comparing Fig. 4a and 4b, we note that the relative permeability of the cylinder substantially affects the structure of the attenuation or scattering efficiency, particularly in the vicinity of the resonance region. Also, the behavior of the attenuation efficiency largely depends on the polarization of the incident radiation, although the resonance effects are observed for any polarization.

The half-width region of the principal resonance peak Q_{ex}^{E} is approximately determined by the conditions $0.6 \le x \le 0.8$ and $80 \le \alpha \le 89.5^{\text{o}}$. Within this region, the attenuation efficiency is much higher than at normal incidence. The polarization of the incident radiation also depends substantially on the radiation scattering. The equalities $Q_{\text{ex}}^{E} = Q_{\text{s}}^{E} = Q_{\text{ex}}^{H} = Q_{\text{s}}^{H}$ in the Fig. 4a and b hold true for the case $m = 1.6$ with a high degree of accuracy. The difference in the last 16th figure appears only at angles of incidence of 85^{o} or higher. It follows, in particular, that for such a refractive index, there is no absorption, in practice, irrespective of the form of polarization and its presence or absence, and also of the diameter of the cylinder and its illumination conditions. The sole exception is the small number of resonance points in the region of large angles of incidence.

Figure 5a demonstrates the process of formation of a resonance peak in the region of small diffraction parameters and large angles of incidence upon the change in the direction of illumination of the cylinder. The results correspond to the case of the relative refractive index $m = 1.6$ which has been also analyzed in [24] in sufficient detail.

The formation of the resonance region of angles of incidence upon the change in the diffraction parameter of the cylinder is shown in Fig. 5b. It follows from this figure that the behavior of the attenuation efficiency largely depends on the polarization of the incident radiation, although the resonance effect may be observed irrespective of polarization.

Local Spectral Characteristics of Ultraporous Materials. The use of the "virtual scanner" [12] turned out to be quite efficient in investigating both the local characteristics and the properties of materials as a whole. In this section, we discuss results obtained when investigating the local spectra of absorption, scattering, and transmission of ultraporous materials with the virtual scanner.

We can observe interesting effects changing the properties of fibers of which the materials consist or the properties of the medium in which the material′s OREs are submerged. If ORE fragments have diameters of the order of several microns or are fabricated from dielectrics, no absorption and scattering resonances occur in the thermal region of the spectrum. The spectra have the form of smooth nonmonotonic dependences. However, if the formed substances are electrically conducting or have a significant imaginary part of permittivity, resonance properties of the spectral coefficients are manifested [18, 19, 24]. Thus, Fig. 6 shows the spectral dependences of the absorption α_λ and scattering β_λ coefficients, the quantum mean free path $l_\lambda = (\alpha_\lambda + \beta_\lambda)^{-1}$, and the spectral-transport coefficient of diffusion of radiation $D_\lambda = 3[\alpha_\lambda + (1 - \langle\cos\theta\rangle)\beta_\lambda]^{-1}$ for OREs of a hypothetical fibrous material having quadratic values of the imaginary part in the permittivity ε compared to the corresponding value in amorphous quartz. Also, Fig. 6 shows the form of the Rosseland spectral function

$$f_\lambda(\tau) = \tau^{-6} e^{-1/\tau} (1 - e^{-1/\tau})^{-3}, \quad \tau = \frac{\lambda k T}{hc} = \lambda T \cdot 69.48028, \tag{4}$$

which is involved in the expression for the radiative component of thermal conductivity [8], thus determining the width of a spectral region significant for heat transfer by radiation. The diameters of cylindrical fragments are marked by rectangles on the horizontal axis.

Note that the ORE absorption and scattering spectra correlate with the equilibrium-radiation curve and with the spectral curves of the constituent substance alike [25]. In the thermal region of the spectrum, of doubtless interest is the transparency peak at a wavelength of ~7.3 μm, which is shown in Fig. 6b. This peak is attributed to the special properties of the constituent substance and is observed for all OREs. It has turned out that the quantity n_{g} is the main factor affecting the

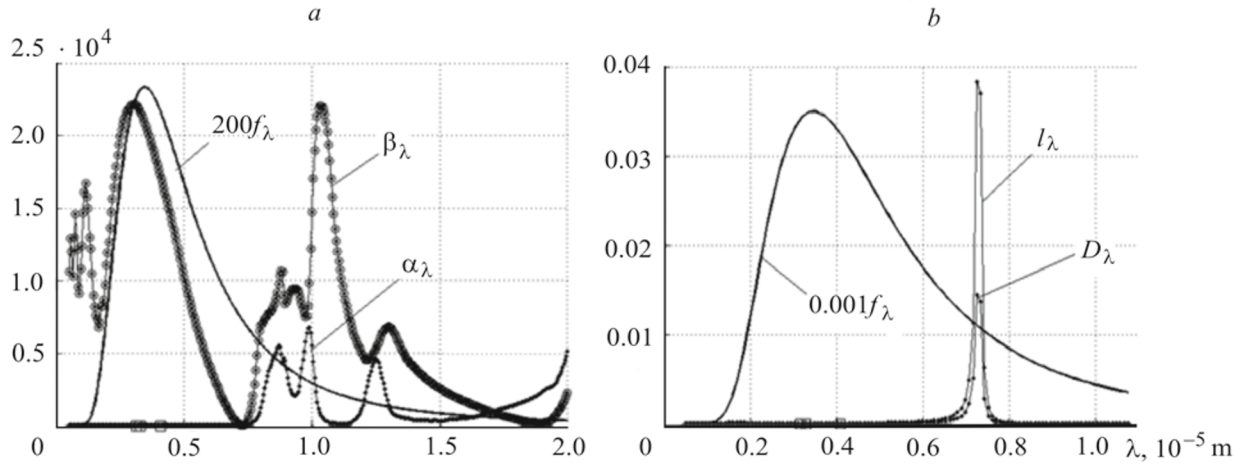

Fig. 6. Spectral weight function f_λ (4) at $T = 700$ K, and also the spectra of the optical absorption α_λ and scattering β_λ coefficients of the OREs (a) and of the coefficient of diffusion of radiation D_λ and the mean free path of photons l_λ (b). The direction of ORE illumination is $\theta_{in} = 60^o$ and $\varphi_{in} = 15^o$. The diameters d and lengths l of cylindrical fragments are $d_x = 3.1422$ μm and $l_x = 29.284$ μm, $d_y = 4.0878$ μm and $l_y = 29.284$ μm, and $d_z = 3.2798$ μm and $l_z = 16.269$ μm. The refractive index of the gas in the pore is $n_g = 1$.

transmission resonance if the properties of the constituent substances of the material′s fragments remain constant. Figure 7 illustrates the dependence of the peak of transmission resonance on the refractive index n_g of the gas filling the pores.

At $\lambda > 7$ μm, the shape of the spectral curves for OREs depends no longer on the diameters of the fragments (in modeling, they did not exceed 5 μm), and the material behaves as a continuous medium. Such behavior in the region of long waves is observed in the spectra of porous materials whose constituent substances are electrically conducting as, e.g., in the case of reticulated vitreous carbon RVC. However, such behavior begins with the wavelengths $\lambda \sim 150$ μm, since bridges between the nodes of its reticulated structure have large diameters [11].

Figure 8 shows analogous results of calculating the absorption, scattering, and transmission spectra for the OREs of reticulated vitreous carbon RVC ETT-CF-ULT at the temperature $T = 1000$ K. In determining the last two quantities, a correction for the effect of induced radiation was introduced into the calculations [7, 10]. It was assumed that the material is operated in vacuum and the character of radiation anisotropy is determined by the distribution (1) with the parameter $g = 0.3$. The direction of illumination and the dimension of the fragments (of the sphere node and three pairs of cylindrical bridges oriented along the coordinate axes) are indicated in the captions to Fig. 8. As we can see, the absorption is resonance-type in character, in practice, and the highest resonance peaks α_λ were cut at $\alpha_{max} = 2 \cdot 10^{12}$ m^{-1} in constructing the plot. Noteworthy is the extremely low spectral albedo of the material′s absorption at the assigned temperature in a spectral region that is far beyond the region of lumped thermal radiation. This is due to the fact that at $T = 1000$ K, vitreous carbon is a semiconductor and has $\varepsilon = 15.4$ m and the comparatively high specific resistance $\rho_e = 4.5 \cdot 10^{-5}$ Ω·m, at which the imaginary part of the complex permittivity is small [1, pp. 359–384; 11].

It should be noted that the low spectral albedo of absorption against the background of substantially stronger scattering is a common property of high-porosity thermal protective materials that restricts considerably the radiative transfer in them. They seem to misguide electromagnetic radiation in the elements of their base because of the strong scattering, and the low absorption restricts the warmup of the base of these elements by radiation, thus diminishing the growth of conductive thermal conductivity.

Clearly, the absorption spectrum of a porous material may be very sensitive to the change in the electrical resistance of its base [18]. Thus, on replacement of vitreous carbon by the hypothetical material with the same specific resistance decreased $k_{\rho_e} \in [0.01; 17.85] \cdot 10^{-2}$ times, we observe a peculiar "order catastrophe" in the absorption spectrum of representative elements at a certain wavelength λ_c in the scanned region $\lambda \in [0.5; 250]$ μm. At this wavelength, we have both a fundamental change in the absolute values of the absorption coefficient (growth of 9 orders of magnitude) and an appreciable qualitative change in the behavior of the plot of $\alpha_\lambda(\lambda)$: it becomes smoother, and resonance peaks appear much more rarely. This process at $k_{\rho_e} = 0.7$ corresponds to $\lambda_c = 98.1$ μm and is shown in Fig. 9.

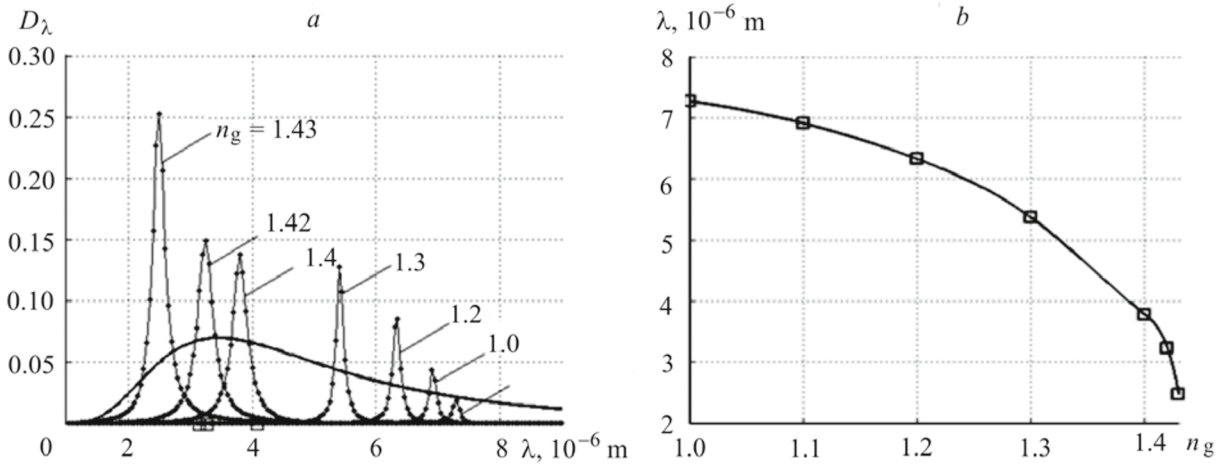

Fig. 7. Transmission resonance vs. refractive index n_g of the gas filling the pores: a) position, peak height, and trend of the Rosseland function (4) at T = 700 K; b) resonance wavelength vs. n_g.

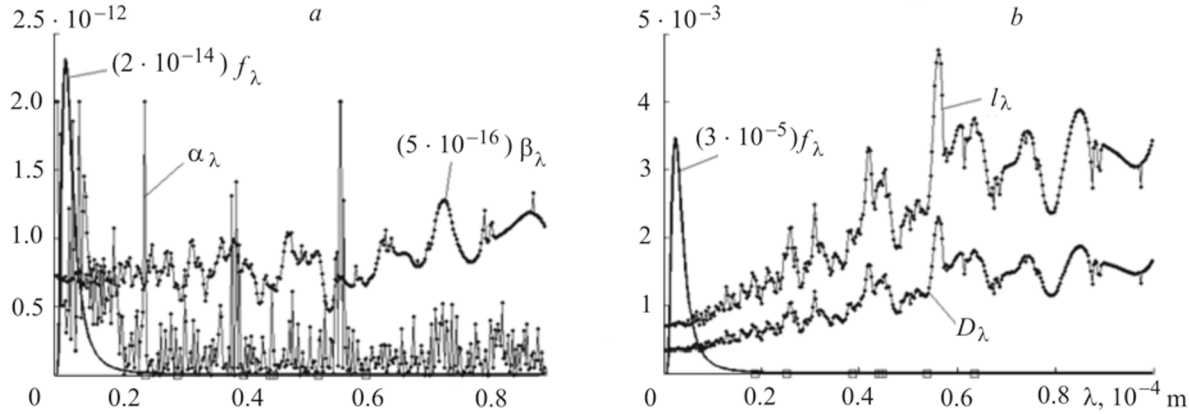

Fig. 8. Function (4) and spectral-kinetic coefficients of one ORE of reticulated vitreous carbon RVC ETT-CF-ULT [11] at T = 1000 K, ε = 15.4, and $\rho_e = 4523 \cdot 10^{-8}$ Ω·m; the direction of illumination is $\theta_{in} = 0.5^o$ and $\varphi_{in} = 15^o$: a) coefficients of absorption α_λ and scattering β_λ of radiation; b) coefficient of diffusion of radiation D_λ and the mean free path of photons l_λ. The scanning pitch is $\Delta\lambda$ = 0.2 μm. The dimensions of the fragments (the diameters are marked on the horizontal axes) are as follows: the node diameter $d_b = 6.3406 \cdot 10^{-5}$ μm and the diameters and lengths of the bridges are $d_{x1} = 4.4683 \cdot 10^{-5}$ μm and $l_{x1} = 2.1641 \cdot 10^{-4}$ μm, $d_{x2} = 5.382 \cdot 10^{-5}$ and $l_{x2} = 1.9807 \cdot 10^{-5}$, $d_{y1} = 4.3867 \cdot 10^{-5}$ and $l_{y1} = 3.3415 \cdot 10^{-5}$, $d_{y2} = 1.8715 \cdot 10^{-5}$ and $l_{y2} = 1.6951 \cdot 10^{-54}$, $d_{z1} = 2.5167 \cdot 10^{-5}$ and $l_{z1} = 1.5524 \cdot 10^{-5}$, $d_{z2} = 3.8645 \cdot 10^{-5}$ and $l_{z2} = 2.5896 \cdot 10^{-4}$. The ORE volume is $dV = 2.696402 \cdot 10^{-11}$ m^3.

With successive decrease in k_{ρ_e}, the quantity λ_c moves from the longwave boundary of the region to the shortwave one. This process obeys the simple relation $\lambda_c = 0.0014 \cdot (k_{\rho_e} = 10^{-4})$. At $k_{\rho_e} = 10^{-4}$ in the entire analyzed spectral region we obtain a fully transformed absorption spectrum (Fig. 10). The "order catastrophe" producing such abrupt changes in the material′s properties may be interpreted as phase transition. An obvious feature of the new state is a certain synchronization of the absorption and scattering spectra, which is not observed on the curves in Fig. 6, obtained for materials consisting of dielectric fragments. Furthermore, spectral curves for such materials demonstrate the "counterphase" in the longwave spectrum: the maximum of the absorption curve corresponds to the minimum of the scattering curve.

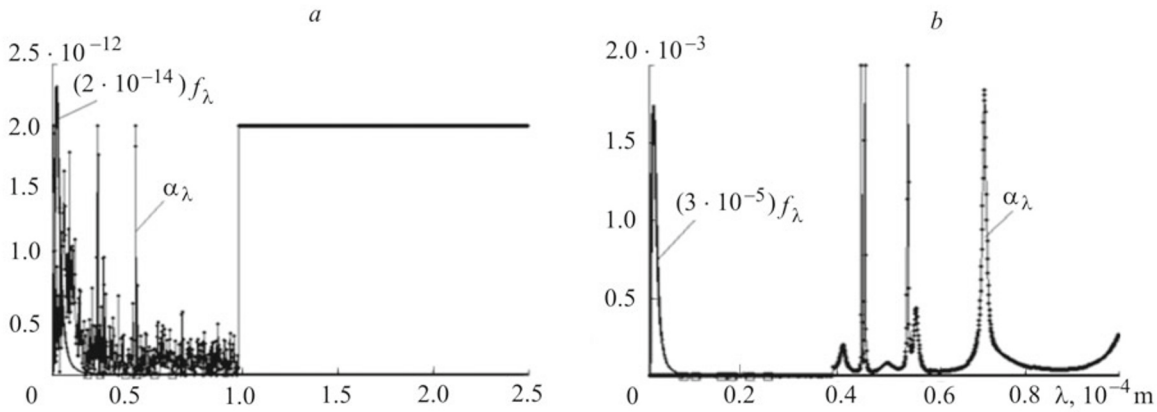

Fig. 9. "Order catastrophe" in the spectrum of absorption α_λ of the OREs of a hypothetical reticulated material at $k_{\rho_e} = 0.07$ ($\lambda_c = 98.1$ μm), $T = 1000$ K, $\varepsilon = 15.4$, and $\rho_e = 4523 \cdot 10^{-8} k_{\rho_e}$ Ω·m: a) the scale of the vertical axis makes it possible to see the shortwave part of the α_λ spectrum; the α_λ values at longer waves are cut at $\alpha_{max} = 2 \cdot 10^{12}$ m^{-1}; b) the α_λ spectrum in the entire scanned region, $\alpha_{max} = 2 \cdot 10^{-3}$ m^{-1}. The direction of illumination is $\theta_{in} = 60.5^o$ and $\varphi_{in} = 15^o$. The dimensions of the fragments and the scanning pitch are the same, as in Fig. 8.

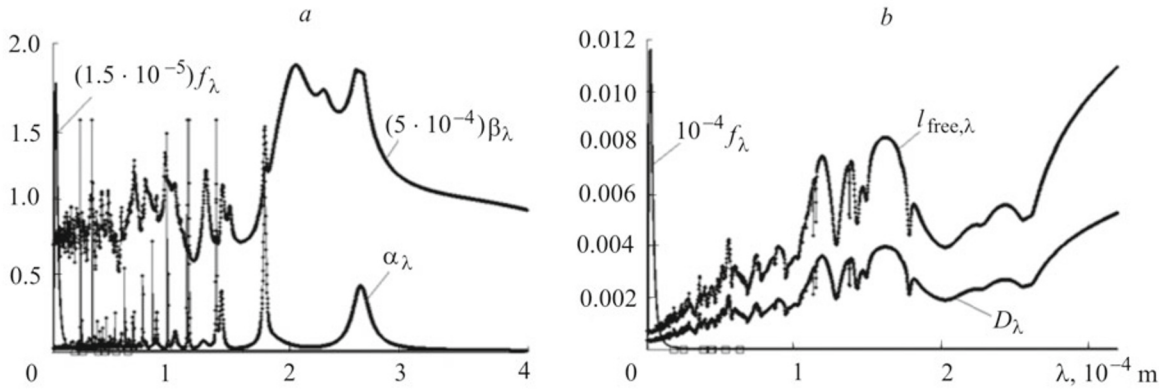

Fig. 10. Behavior of the spectral-kinetic coefficients of a hypothetical reticulated material at $k_{\rho_e} = 10^{-4}$.

Note that the effect of the "order catastrophe" was only observed as the reaction to a purely formal change in the electrical resistance of the constituent substance. Certainly, it may also be of interest from the applied viewpoint. However, even in the spectra of porous materials whose constituent substance is electrically conductive, such as abrupt change in the properties is not always observed and strongly depends on the initial level of specific electrical resistance. For example, the absorption spectrum may be purely resonance-type in character up to the wavelength $\lambda = 400$ μm (large λ values were not analyzed). Furthermore, it may occur that the Kramers–Kronig relations [19], which establish relations between spectral refractive and absorption indices (material coefficients), will restrict or even fully eliminate such effects in actual practice. However, this relationship between the observed result of modeling and the fundamental constraints on material coefficients formulated for the full spectrum has not been investigated.

Conclusions. We have developed an efficient mathematical model for investigating the characteristics of high-temperature nonmetallic ultraporous materials and a number of physical properties occurring in them on a varying spatial and temporal scale. The model was used to investigate the local and global spectral properties for representatives of the classes of materials, which are relevant and advanced from the applied viewpoint. Results confirming the adequacy of the spectral model have been given.

We have obtained the typical spectra of absorption, scattering, and transmission of representative elements of the materials. The effect of the "order catastrophe" in the absorption spectrum of reticulated materials upon the change in the specific electrical resistance of the material of the base has been found and investigated. With this effect, a strong abrupt change (a change of nine orders of magnitude was recorded) in the spectral absorption index, which is not associated with the resonance phenomena, is observed in the scanned region of the spectrum. We have shown the presence of the spectral transparency region in the transmission spectra of the amorphous-quartz-based fibrous material, determined the influencing parameter, and investigated the effect of shift of the region upon its change.

Acknowledgment. This work was carried out with financial support from the Russian Science Foundation within the framework of Project No. 18-19-00492.

NOTATION

a, anisotropic index of the material; *D*, spectral-transport coefficient of diffusion of radiation; D, dispersion; *d*, diameter; *dV*, volume of the representative element; *F*, distribution law; *g*, Henji–Greenstein distribution parameter; k_{ρ_e}, factor of the specific electrical resistance; *l*, length of the fiber (bridge) of a volume element, the photon mean free path; M, mathematical expectation; *m*, complex relative refractive index of a scattering body; *P*, probability; *Q*, spectral efficiency; *x*, diffraction parameter; *y*, variable; α, angle of incidence of radiation (Fig. 4); α and β, coefficients of absorption and scattering of radiation; ε and μ, relative permittivity and permeability; λ, wavelength; ρ, effective mass density, the specific electrical resistance; σ, standard deviation; ψ, probability density. Subscripts: $\langle ... \rangle$, average; b, sphere (node), inverse; *E* and *H*, independent polarization states; e, electrical; HG, Henji–Greenstein distribution; in, incident; λ, spectral.

REFERENCES

1. B. S. R. Reddy (Ed.), *Advances in Nanocomposites — Synthesis, Characterization and Industrial Applications*, Rijeka, Croatia (2011). ISBN: 978-953-307-165-7.
2. S. A. Meguid (Ed.), *Advances in Nanocomposites: Modeling, Characterization and Applications*, Springer International Publishing, Switzerland (2016); DOI: 10.1007/978-3-319-31662-8.
3. E. Placido, M. C. Arduini-Schuster, and J. Kuhn, Thermal properties predictive model for insulating foams, *Infrared Phys. Technol*., **46**, No. 3, 219–231 (2005).
4. J. Petrasch, P. Wyss, and A. Steinfeld, Tomography-based Monte Carlo determination of radiative properties of reticulate porous ceramics, *J. Quant. Spectrosc. Radiat. Transf*., **105**, 180–197 (2007).
5. O. M. Alifanov, S. A. Budnik, V. V. Mikhaylov, A. V. Nenarokomov, D. M. Titov, and V. M. Yudin, An experimental-computational system for materials thermal properties determination and its application for spacecraft structures testing, *Acta Astronautica*, **61**, Nos. 1–6, 341–351 (2007); http://dx.doi.org/10.1016/j.actaastro.2007.01.035.
6. A. Öchsner, G. E. Murch, and M. J. S. de Lemos (Eds.), *Cellular and Porous Materials: Thermal Properties Simulation and Prediction*, Wiley-VCH, Weinheim (2008); http://dx.doi.org/10.1002/9783527621408.
7. R. Coquard, D. Rochais, and D. Baillis, Experimental investigation of the coupled conductive and radiative heat transfer in metallic/ceramic foams, *Int. J. Heat Mass Transf*., **52**, Nos. 21–22, 4907–4918 (2009).
8. O. M. Alifanov and V. V. Cherepanov, Mathematical simulation of high-porosity fibrous materials and determination of their physical properties, *High Temp*., **47**, No. 3, 438–447 (2009); http://dx.doi.org/10.1134/S0018151X09030183.
9. J.-F. Sacadura, Thermal radiative properties of complex media: theoretical prediction versus experimental identification, *Heat Transf. Eng*., **32**, 754–770 (2011).
10. D. Rochais, R. Coquard, and D. Baillis, Microscopic thermal diffusivity measurements of ceramic and metallic foams lumps in temperature, *Int. J. Therm. Sci*., **98**, 179–187 (2015); http://dx.doi.org/10.1016/j.ijthermalsci.2015.01.027.
11. O. M. Alifanov, V. V. Cherepanov, and A. V. Morzhukhina, Complex study of the physical properties of reticulated vitreous carbon, *J. Eng. Phys. Thermophys*., **88**, No. 1, 134–144 (2015); http://dx.doi.org/10.1007/s10891-015-1175-9.
12. V. V. Cherepanov, O. M. Alifanov, A. V. Morzhukhina, and A. V. Cherepanov, Interaction of radiation with orthogonal representative elements of highly porous materials, *Appl. Math. Model*., **40**, Nos. 1–2, 3459–3474 (2016); http://dx.doi.org/10.1016/j.apm.2015.03.040.
13. R. A. Mironov, M. O. Zabezhailov, M. Yu. Rusin, and V. V. Cherepanov, Calculation of the optical properties of quartz ceramics based on data on its structure, *High Temp*., **56**, No. 1, 44–51 (2018); http://dx.doi.org/10.1134/S0018151X1706013X.

14. R. A. Mironov, M. O. Zabezhailov, V. V. Cherepanov, and M. Yu. Rusin, Transient-radiative-conductive heat transfer modeling in constructional semitransparent silica ceramics, *Int. J. Heat Mass Transf.*, **127**, 1230–1238 (2018); https://doi.org/10.1016/j.ijheatma2018.08.052.
15. M. F. Modest, *Radiative Heat Transfer*, third ed., Academic Press, Elsevier Science, New York (2016); http://dx.doi.org/10.1016/B978-0-12-386944-9.50028-5.
16. J. R. Howell, M. P. Mengüç, and R. Siegel, *Thermal Radiation Heat Transfer*, sixth ed., Taylor & Francis Group, LLC, Boca Raton (2016).
17. S. Chapman and T. G. Cowling, *The Mathematical Theory of Non-Uniform Gases*, second ed., Cambridge University Press, Cambridge (1952).
18. J. D. Jackson, *Classical Electrodynamics*, Wiley, New York (1962).
19. C. F. Bohren and D. R. Huffman, *Absorption and Scattering of Light by Small Particles*, Wiley, New York (1998).
20. O. M. Alifanov, *Inverse Heat Transfer Problems*, Springer, Berlin, New York (1994); http://dx.doi.org/10.1007/978-3-642-76436-3.
21. S. M. Ermakov, Die Monte Carlo Methode und verwandte Fragen, Oldenbourg Verlag, Munich–Vienna (1975).
22. D. P. Kroese, T. Taimre, and Z. I. Botev, *Handbook of Monte Carlo Methods*, Wiley, Hoboken, New Jersey (2011). ISBN: 978-0-470-17793-8.
23. K. N. Liou, *An Introduction to Atmospheric Radiation*, second ed., Elsevier — Academic Press, New York, London (2002). ISBN: 0-12-451451-0.
24. A. C. Lind and J. M. Greenberg, Electromagnetic Scattering by obliquely oriented cylinders, *J. Appl. Phys.*, **37**, 3195–3203 (1966); DOI: http://dx.doi.org/10.1063/1.1703184.
25. D. Banner, S. Klarsfeld., and C. Langlais, Temperature dependence of the optical characteristics of semitransparent porous media, *High Temp.–High Press*., **21**, 347–354 (1989); http://www.oldcitypublishing.com/journals/hthp-electronic-archive-home/hthp-electronic-archive-issue-contents/.